Journal of Power Sources 328 (2016) 151–160

Contents lists available at ScienceDirect

Journal of Power Sources

journal homepage: www.elsevier.com/locate/jpowsour

Selection of optimal sensors for predicting performance of polymer electrolyte membrane fuel cell

Lei Mao*, Lisa Jackson

Department of Aeronautical and Automotive Engineering, Loughborough University, Leicestershire, LE11 3TU, UK

HIGHLIGHTS

- Performance of sensor selection algorithms in PEM fuel cell prognosis is studied.
- Sensor sensitivity to fuel cell failures is calculated for the sensor selection.
- Proposed selection approach considers sensor sensitivity and noise resistance.
- Reliable prediction can be made with optimal sensors from proposed approach.

ARTICLE INFO

Article history:
Received 13 June 2016
Received in revised form
2 August 2016
Accepted 3 August 2016

Keywords:
Sensor selection approaches
PEM fuel cell
Sensitivity analysis
Performance prediction
Adaptive neuro-fuzzy inference system

ABSTRACT

In this paper, sensor selection algorithms are investigated based on a sensitivity analysis, and the capability of optimal sensors in predicting PEM fuel cell performance is also studied using test data. The fuel cell model is developed for generating the sensitivity matrix relating sensor measurements and fuel cell health parameters. From the sensitivity matrix, two sensor selection approaches, including the largest gap method, and exhaustive brute force searching technique, are applied to find the optimal sensors providing reliable predictions. Based on the results, a sensor selection approach considering both sensor sensitivity and noise resistance is proposed to find the optimal sensor set with minimum size. Furthermore, the performance of the optimal sensor set is studied to predict fuel cell performance using test data from a PEM fuel cell system. Results demonstrate that with optimal sensors, the performance of PEM fuel cell can be predicted with good quality.

1. Introduction

In the last few decades, with the fast application of fuel cells in many areas, including stationary power, automotive, and consumer electronics, the reliability and durability of fuel cells during their operation have attracted more attention, leading to several studies in the field of diagnostics and prognostics of fuel cells.

From previous research, a series of studies have been devoted for fuel cell fault diagnostics to detect and isolate fuel cell faults, including model-based approaches and those with a data-driven framework. With model-based approaches, a numerical model is developed, which should express the fuel cell system performance with consideration of the failure mechanisms, and residuals between model outputs and actual measurements can be used to identify and isolate the fuel cell faults [1–10]. For data-driven techniques, signal processing techniques are applied to the sensor measurements to extract features expressing fuel cell performance, and by classifying these features, different fuel cell failure modes can be determined, such as fuel cell flooding, drying out, carbon corrosion, etc. [11–21].

Compared to fuel cell fault diagnosis, only limited research has been performed in fuel cell prognostics to predict the fuel cell performance and its remaining useful life (RUL). Several studies [22–24] proposed an adaptive neuro-fuzzy inference system (ANFIS) to predict the fuel cell system performance, which combined the advantages of a neural network and fuzzy logic system. With the developed ANFIS, fuel cell outputs, such as voltage and efficiency, could be predicted. Moreover, particle filtering approach has also been applied to update the state of the fuel cell system [25], and with predicted fuel cell voltage and threshold values, the remaining useful life (RUL) could be decided.

It can be noticed that the training process is required in most studies to predict the fuel cell performance, thus the prediction

* Corresponding author.
E-mail address: l.mao@lboro.ac.uk (L. Mao).

http://dx.doi.org/10.1016/j.jpowsour.2016.08.021

performance relies largely on the quality of sensor measurements. As a set of sensors is usually installed in the practical fuel cell system, including sensors at the fuel cell anode and cathode sides for collecting different information such as temperature, flow rate, pressure, humidity, etc., and these sensors may have different sensitivities to the fuel cell performance variation, it is not necessary to involve all these sensors in the analysis, which may increase the computation time, fuel cell system complexity and cost. Moreover, the existence of environment/measurement noise may also mask the contributions of sensors, especially those with low sensitivity. On this basis, a sensor selection algorithm should be applied to find the optimal sensors, which can provide reliable predictions with minimum computation time.

According to previous research, several studies have investigated selection of the optimal sensor set for health management of various systems, and the algorithms for sensor selection include generation of an objective function with performance requirements [26–28], and evaluation of sensor performance using sensitivity-related analysis [29]. However, although several studies have been carried out to investigate the sensitivity of PEM fuel cell parameters [30–34], including stack temperature, pressure, relative humidity, etc. on the PEM fuel cell performance, few studies have been devoted to the sensor selection technology for fuel cell health management which requires further investigation with the wide application of fuel cells in practical applications.

This paper presents the approaches for selecting optimal sensors based on the sensitivity analysis, and the capability of optimal sensors in predicting PEM fuel cell performance is also studied. Section 2 determines the fuel cell health parameters which are critical to the PEM fuel cell performance. In section 3, the fuel cell model is developed and its performance is validated using test data. Based on the developed fuel cell model, the sensitivity matrix is generated to relate sensor measurements and fuel cell health parameters, which is described in section 4. Section 5 presents three sensor selection approaches, including the largest gap method, exhaustive brute force searching method, and the proposed approach considering both sensor sensitivity and noise resistance, the selection results from these techniques are also compared in this section. In section 6, the performance of optimal sensors in predicting PEM fuel cell performance is studied using test data from a PEM fuel cell system. From the findings, conclusions will be given in section 7.

2. Determination of fuel cell health parameters

Before evaluating sensor sensitivities to fuel cell performance variation, the health parameters should be selected, which can represent different fuel cell failure modes. Theoretically, the number of health parameters should be minimized to reduce the computation cost. Based on previous studies [35–37], some typical failure modes of the fuel cell and corresponding health parameters can be determined, which are listed in Table 1.

From Table 1, it can be seen that some health parameters can express more than one failure mode, such as ECSA, the amount of water inside the fuel cell, etc., which indicates that extra information is required to isolate the degraded components when performing fault diagnostics with these health parameters.

Moreover, as performing sensitivity analysis using experimental studies is time-consuming and costly, a numerical fuel cell model is developed in this study to determine the relationship between health parameters and sensor measurements. From previous studies [38], as membrane and electrodes are the most critical components in PEM fuel cells, the health parameters related to these components are selected in the analysis, including membrane resistance, internal current, and ECSA. Moreover, since fuel cell flooding can cause the most rapid performance degradation [39], the amount of water inside the fuel cell is also included in this study. Therefore, the health parameters selected in sensitivity analysis include membrane resistance, internal current, ECSA, and the amount of water inside the fuel cell.

3. Development of fuel cell model and its performance validation

In this paper, a numerical fuel cell model is developed to perform the sensitivity analysis. In the model, the anode and cathode are modelled separately as lumped volumes, the mass of each gas is calculated from the 1st order differential mass balances in Eqs. (1)–(5), fuel cell temperature is calculated using a single thermal capacitance model shown in Eq. (6), and fuel cell voltage can be calculated with Eq. (7) using results from Eqs. (1)–(6). More details can be found in Refs. [40–42]. The block diagram of the fuel cell model is depicted in Fig. 1.

Anode side

$$\frac{dm_{H_2}}{dt} = W_{H_2,in} - W_{H_2,out} - W_{H_2,react} \tag{1}$$

$$\frac{dm_{H_2O}}{dt} = W_{H_2O,in} - W_{H_2O,out} + W_{H_2O,trans} \tag{2}$$

Cathode side

$$\frac{dm_{N_2}}{dt} = W_{N_2,in} - W_{N_2,out} \tag{3}$$

$$\frac{dm_{O_2}}{dt} = W_{O_2,in} - W_{O_2,out} - W_{O_2,react} \tag{4}$$

$$\frac{dm_{H_2O}}{dt} = W_{H_2O,in} + W_{H_2O,react} - W_{H_2O,out} - W_{H_2O,trans} \tag{5}$$

where m is the mass of gas species, W is the mass flow rate, *in* shows the inlet species, *out* shows the outlet species, *react* is the electrochemical reaction energy, and *trans* is the transport loss.

Energy balance

$$m_{stack}C_{ps}\frac{dT}{dt} = Q_{react} - Q_{elec} + Q_{in} - Q_{out} - Q_{loss} \tag{6}$$

where T is the fuel cell stack temperature, T^0 is ambient temperature (293 K in the model), the m_s is the mass of fuel cell stack, C_{ps} is the specific heat, $Q_{react} = \Delta\widehat{h_{H_2}} \cdot \dot{m_{H_2 in}}$ is the heat released during the reaction ($= \Delta\widehat{h_{H_2}}$ is the entropy change of hydrogen, $\dot{m_{H_2\ in}}$ is the inlet hydrogen mass flow rate), $Q_{elec} = V_{stack}I_{stack}$ is the electrical power generated by the fuel cell stack, $Q_{in} = Q_{H_2in} + Q_{N_2in} + Q_{O_2in} + Q_{H_2o\ liquid\ in} + Q_{H_2o\ vapour\ in}$ and $Q_{out} = Q_{N_2out} + Q_{O_2\ out} + Q_{H_2o\ vapour\ out}$ are the heat flows into and out of the fuel cell stack, $Q_{loss} = h_{stack}A_{stack}(T_{stack} - T^0)$ is a term to represent the small amount of energy lost from the fuel cell stack surface (h_{stack} stack convective heat transfer coefficient, A_{stack} is the stack area), H_v is the enthalpy of water vapour.

With results from the above equations, the fuel cell voltage can be calculated as follows.

$$V_{cell} = E_n - V_{act} - V_{FC} - V_{trans} - V_{ohm} \tag{7}$$

where V_{cell} is the single cell voltage, E_n is the reversible voltage, $V_{act} = \frac{RT}{2\alpha F}\ln\left(\frac{i}{i_{oc}}\right)$, $V_{FC} = \frac{RT}{2\alpha F}\ln\left(\frac{i_n}{i_{oc}}\right)$, $V_{trans} = m_{trans}.e^{n_{trans}.i}$, $V_{ohm} = i.R_{membrane}$ are the activation loss, fuel crossover loss, mass

Table 1
Typical fuel cell failure modes and corresponding health parameter.

Component	Failure mode	Corresponding health parameter
Membrane	Dehydration/drying	Membrane resistance
	Pinhole/crack	Internal current
Catalyst layer (CL)	Pt growth/dissolution	Electrochemical surface area (ECSA)
	Carbon corrosion	ECSA
		Carbon dioxide
	Air/fuel impurities	ECSA
	Deformation of catalyst structure	ECSA
	Porosity loss	Water amount inside fuel cell
	Flooding	Water amount inside fuel cell
Gas diffusion layer (GDL)	Loss of porosity and gas permeability	Water amount inside fuel cell
Bipolar plates (BP)	Corrosion (affect membrane/CL/GDL)	Membrane resistance
		ECSA
		Contact resistance
	Mechanical defects	Reactant leakage

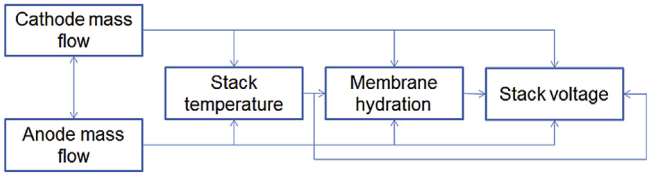

Fig. 1. Block diagram of developed fuel cell model.

transport loss, and Ohmic loss, respectively (R is universal gas constant, α is charge transfer coefficient, F is Faraday constant, i_{oc} is exchange current density at cathode, i_n is the interal current density, m_{trans} and n_{trans} are the mass transport loss voltage coefficients, $R_{membrane}$ is the membrane resistance), which can be calculated using results from Eqs. (1)–(6).

It should be mentioned that several assumptions are used for the model development. At the anode side, the nitrogen diffusion through the membrane is not considered in the model; the temperature in the anode and cathode volumes is assumed as the same as the stack temperature; uniform temperature distribution is assumed throughout the stack; and products exiting the stack is assumed at the stack temperature.

With the developed model, the cell voltage can be determined in the 'stack voltage' module using Eq. (7) with results from other modules, hydration is calculated in the 'membrane hydration' module, the anode and cathode mass balance equations are calculated in the 'anode model' and 'cathode model' with Eqs. (1)–(5), and energy balance is determined in the 'stack temperature' module using Eq. (6). It should be mentioned that the current is fed into the model and is the determining factor in the calculations. The 'membrane hydration' module uses the results of the mass balance equations to calculate the resistance of the membrane, and feeds back data into the anode and cathode mass balance modules. The determined resistance values feed directly into the 'stack voltage' module, while the 'stack temperature' module takes outputs from all of the other modules for its calculations.

Before performing the sensitivity analysis, the performance of the developed fuel cell model is validated using test data from a fuel cell system. In this study, the fuel cell tested in Ref. [41] can be simulated by configuring model parameters listed in Table 2. With the configured fuel cell model, the polarization curve at different operating conditions can be obtained and compared with that in the reference paper [41], which is depicted in Fig. 2. It should be noted that the parameter values from semi-empirical model in Ref. [41], including internal and exchange current densities, mass transport coefficients, etc. are used in the developed fuel cell model to simulate the tested PEM fuel cell.

Table 2
Input parameters for fuel cell model from Ref. [41].

Parameter (unit)	Value
Number of fuel cells	1
Active electrode area of single cell (cm^2)	25
Hydrogen flow rate (slpm)	0.2
Air flow rate (slpm)	0.2
Hydrogen pressure (bar)	1
Air pressure (bar)	1

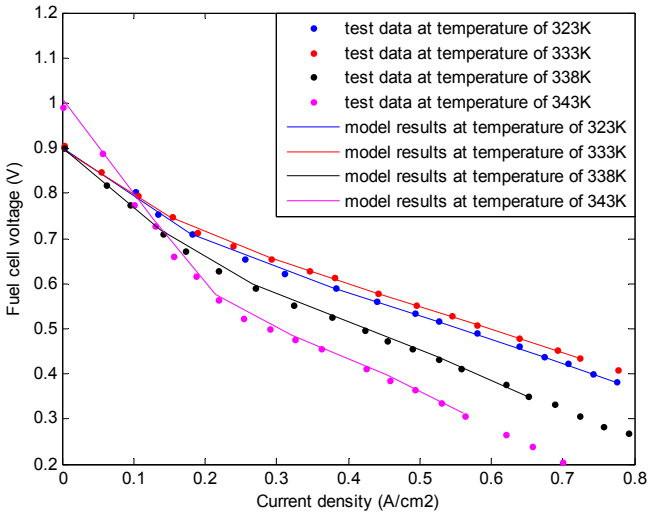

Fig. 2. Comparison of polarization curves from the model and test in Ref. [41] at different temperatures.

From the results, the measured polarization curves from the tests at different operating conditions can be simulated with good quality with the developed fuel cell model, and the difference between numerical and test data is less than 2%, which is obtained by calculating the difference between the simulated fuel cell voltage and test voltage at same current densities.

With the validated fuel cell model, the relationship between sensor measurements and fuel cell health parameters can be determined by generating a sensitivity matrix, which can also be used to evaluate the sensor resistance to measurement noise.

4. Generation of sensitivity matrix

In this section, the sensitivity matrix relating fuel cell sensor

measurements to health parameters will be determined using the developed fuel cell model. In the analysis, a certain change (1% increase used herein) is applied to the fuel cell health parameters in the numerical model, and the variations in fuel cell responses (sensor outputs) are obtained. It should be noted that sensors used in this paper are determined with consideration of sensor availability in the practical fuel cell system and the physical fuel cell model, including cell voltage, inlet and outlet flow at the anode and cathode, stack temperature, etc., which are listed as sensor outputs in Table 3. Moreover, in order to determine the sensor sensitivity to each health parameters, in the analysis, only one health parameter is to be changed in each case. The results are then transferred to the sensitivity values using Eq. (8), and the sensitivities of fuel cell sensors to selected parameters are listed in Table 3.

$$S_{ij} = \frac{Rj_2 - Rj_1}{Pi_2 - Pi_1} \tag{8}$$

where S represents the sensitivity value, R is the sensor reading, P is the selected fuel cell health parameter, 1 and 2 represent values before and after applying the certain change, Sij is the jth sensor sensitivity for the ith health parameter.

It should be mentioned that the sensor sensitivities to internal current are not listed in Table 3, as all the sensors will give zero sensitivities to the internal current variation. The reason proposed is that the internal current value is much smaller compared to the other health parameters (3.55×10^{-41} A/cm^2 used in the model), thus its change doesn't lead to a clear variation in the sensor outputs. Hence, in this study, the effect of internal current will not be further considered.

For comparison purposes, the sensitivity values of fuel cell voltage is normalized to a unit value, and sensitivities of the other sensors to the same health parameter (each column in Table 3) will be changed accordingly. By doing so, the sensitivity of each sensor to various health parameters can be compared directly, and the results are listed in Table 4.

It can be seen that several sensors, including anode inlet mass flow meter, compressor temperature sensor, and coolant inlet mass flow meter, have zero sensitivities to all the health parameters, indicating that these sensors could not make contributions in predicting the fuel cell performance, therefore, they should be excluded from the optimal sensor set.

From results in Table 4, the sensors can be ranked based on their sensitivity values, which can express their responses to fuel cell performance due to different failure modes. The results can be used for selecting the optimal sensors in the following section.

5. Investigation of sensor selection approaches

In this section, three sensor selection approaches will be applied based on the generated sensitivity matrix, including the largest gap method, exhaustive brute force search technique, and the proposed sensor selection algorithm. The details and results of these selection approaches will be presented in the following parts.

5.1. The largest gap method

The largest gap method has been applied to find the size of optimal sensor set for several systems in previous studies [43]. In this method, the sensors should be ranked based on the sensitivity variance values, which can express sensor capability of discriminating various failure modes. Moreover, the size of optimal sensor set can be determined by finding the largest value of ratios between two neighbouring variances.

Table 5 lists the sensors and corresponding sensitivity variance (variance of each row in Table 4), and the ratios of two neighbouring variances are depicted in Fig. 3. It should be noted that sensors with zero sensitivities to all the failure modes are not included in the analysis.

It can be seen from Fig. 3 that although the largest gap exists between sensor 1 and sensor 4, only 1 sensor cannot provide complete information of the fuel cell system (shown in Fig. 6(a)), thus the second largest gap is used in this study, and the optimal sensor set contains 4 sensors (s1, s4, s5 and s2 listed in Table 5).

5.2. Exhaustive brute force searching method

In this section, the optimal sensors will be selected by searching all the possible sensor combinations. It should be mentioned that this approach is very time-expensive, thus it should not be used in the practical applications, and use of this approach herein is to validate the proposed sensor selection method presented in the next section.

In the analysis, the performance of various sensor sets is evaluated with the adaptive neuro-fuzzy inference system (ANFIS), and test data from a PEM fuel cell is used for the searching process.

5.2.1. Description of fuel cell test data

In the analysis, the PEM fuel cell test data from IEEE 2014 data challenge are used, which is open source data [44]. Sensor measurements from the fuel cell system include fuel cell voltage (shown in Fig. 4(a)), current (shown in Fig. 4(b)), anode and cathode inlet and outlet flow, pressure, and temperature. It should be mentioned that during the fuel cell operation, constant current is applied, which gives the steady state of the fuel cell system. Moreover, fuel cell fault is not observed, which means the degradation of fuel cell performance is due to fuel cell aging.

Table 3
Sensitivities of sensors to selected parameters.

Sensor output	Health parameter		
	Membrane resistance (Ω/cm^2)	Cell active area (m^2)	Liquid water inside cell (kg)
Cell voltage (V)	0.3208	0.0011	1.01×10^{-5}
Stack temp (K)	5.5031	0.007	0.0172
Anode inlet flow (kg/s)	0	0	0
Cathode inlet flow (kg/s)	0.0055	1.7×10^{-5}	3.2×10^{-5}
Anode outlet flow (kg/s)	1.7×10^{-5}	7×10^{-8}	1.3×10^{-7}
Cathode outlet flow (kg/s)	0.0047	1.6e-5	3.9×10^{-4}
Compressor temp (K)	0	0	0
Coolant inlet flow (kg/s)	0	0	0
Inlet water temp (K)	0.0786	0.0013	2.0×10^{-4}
Outlet water temp (K)	0.0786	2.0×10^{-4}	0

Table 4
Sensitivity of sensors to selected parameters (after cell voltage normalization).

Sensor output	Health parameter		
	Membrane resistance (Ω/cm^2)	Cell active area (m^2)	Liquid water inside cell (kg)
Cell voltage (V)	1	1	1
Stack temp (K)	17.1543	6.3636	1.7×10^3
Anode inlet flow (kg/s)	0	0	0
Cathode inlet flow (kg/s)	0.0171	0.0155	3.2
Anode outlet flow (kg/s)	5.4×10^{-5}	6.4×10^{-5}	0.0132
Cathode outlet flow (kg/s)	0.0147	0.0145	38.5
Compressor temp (K)	0	0	0
Coolant inlet flow (kg/s)	0	0	0
Inlet water temp (K)	0.245	1.1818	20
Outlet water temp (K)	0.245	0.1818	0

Table 5
Sensor candidates and corresponding sensitivity variance.

Sensor	Sensitivity variance
Stack temperature (s1) (K)	976.3379
Cathode inlet flow (s2) (kg/s)	1.8381
Anode outlet flow (s3) (kg/s)	0.0076
Cathode outlet flow (s4) (kg/s)	22.2196
Water inlet temperature (s5) (K)	11.145
Water outlet temperature (s6) (K)	0.1123

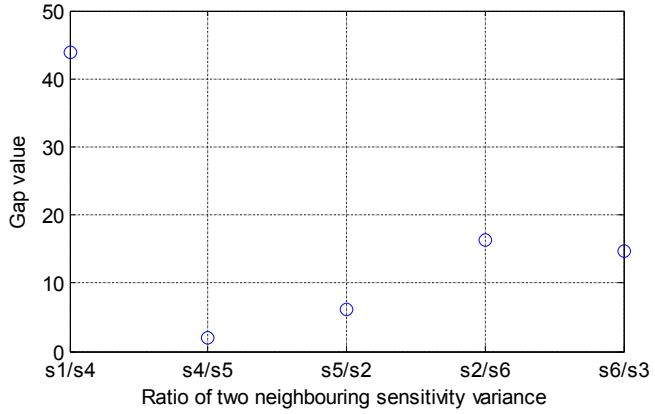

Fig. 3. Distribution of the ratio of two neighbouring sensitivity variance (where si/sj is the variance ratio between si and sj listed in Table 5).

5.2.2. Description of the adaptive neuro-fuzzy inference system

In this study, an adaptive neuro-fuzzy inference system (ANFIS) is used to evaluate the performance of the selected sensors, which has already been proved to be effective in predicting fuel cell performance [22–24]. ANFIS is a multi-layer feed forward neural network, which combines fuzzy rule to improve its inference ability. A typical ANFIS is shown in Fig. 5, which includes five layers. Layer 1 is the fuzzification layer which performs fuzzification to the incoming inputs. For example, two inputs (x_1,x_2) and 4 membership functions (P_{11}, P_{21}, P_{12}, P_{22}) are applied in Fig. 5, formulating 16 rules (2^4) (if-then rule), and the output from layer 1 can be written as in Eq. (9),

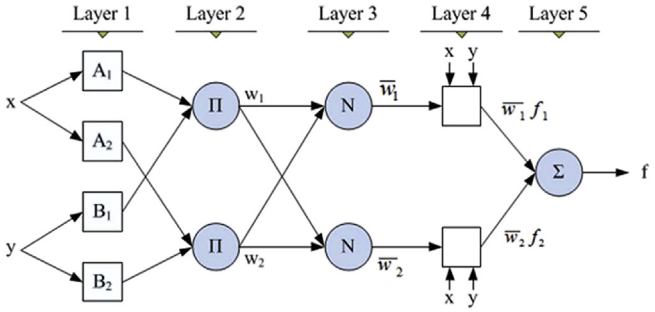

Fig. 5. A typical ANFIS.

$$y_i^1 = \mu_{A_i^j}\left(x_i^1\right) = \frac{1}{1 + \left|\frac{x_i^1 - c_i}{a_i}\right|^{2b_i}} \tag{9}$$

Where $\mu_{A_i^j}$ is the fuzzy rule associated with *ith* input and *jth* fuzzy rule, y_i^1 is the *ith* output at layer 1, a_i, b_i and c_i are the parameters in the membership function, which will be adjusted during the training phase.

In layer 2, the firing strength of the fuzzy rule will be generated, with output y_i^2 from layer 2, which is described in Eq. (10)

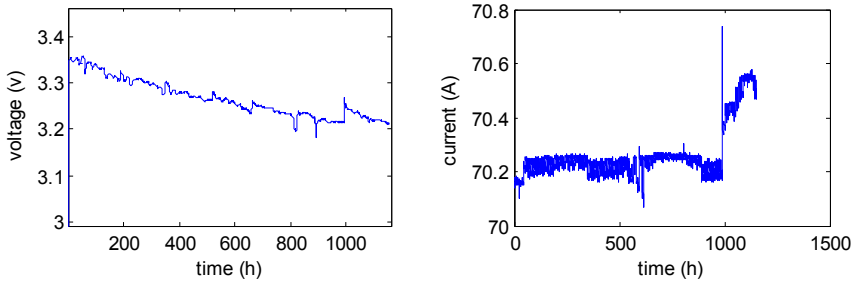

(a) Fuel cell voltage (b) Current

Fig. 4. Fuel cell voltage and current from IEEE data challenge 2014 [44].

$$y_i^2 = \omega_i = \prod_i \mu_{A_i^j}\left(x_i^1\right) \tag{10}$$

Layer 3 is usually defined as the normalization layer, the neurons at this layer receive inputs from all neurons at layer 2 and calculate the normalized firing strength, which can be expressed as y_i^3 in Eq. (11)

$$y_i^3 = \overline{\omega_i} = \frac{\omega_i}{\sum_1^i \omega_i} \tag{11}$$

where ω_i is the firing strength of the rule.

Layer 4 is called the defuzzification layer, each neuron at this layer receives outputs from layer 3 as well as the original inputs of the system (x_1,x_2) for the calculation, with output calculated by Eq. (12)

$$y_i^4 = \overline{\omega_i} f_i = \overline{\omega_i}\left(c_1^j x_1 + c_2^j x_2 + c_3^j\right) \tag{12}$$

where c_1^j, c_2^j and c_3^j are consequent parameters of the *jth* fuzzy rule, which will be updated during the training process.

With outputs from layer 4, the system output can be calculated with Eq. (13)

$$y_i^5 = \sum_i \overline{\omega_i} f_i \tag{13}$$

In the analysis, the inputs of the ANFIS are the measurements from selected sensors, and the output is the fuel cell voltage. The first 2/3rd of the data samples are used to train the ANFIS system, while the last 1/3rd of the data samples are used to validate the performance of selected sensors.

5.2.3. Determination of optimal sensor set

In the analysis, the sensor used in the fuel cell system can be selected from all possible sensors used in the test (with total number of 16, which is listed in Table 6). Based on the above sensor selection results, four sensors are selected for predicting the fuel cell performance. The objective function is defined with the difference between actual fuel cell voltage and corresponding prediction, which can be expressed as:

$$f(x) = \sum_i abs(v_i - p_i) \tag{14}$$

where v_i is the actual fuel cell voltage, and p_i is the corresponding prediction.

The optimal sensor set can be determined by minimizing Eq. (14) with the smallest size of sensor set.

Table 7 lists the optimal sensor sets with minimized objective function, it should be noted that several sensor sets have similar objective function values, indicating these sensor sets can provide similar prediction performance.

Table 7
Selected sensors from exhaustive searching technique.

Sensor set	Objective function value
Tout,an, Win,ca, Wout,ca	0.0132
Tin,ca, Win,ca, Wout,ca	0.0135
Tout,ca, Win,ca, Wout,ca	0.0135
Tin,an, Win,ca, Wout,ca	0.0136

It can be seen from Table 7 that sensor set with only three sensors can give reliable prediction of fuel cell voltage. When compared to the results in section 5.1, water inlet temperature is not included in the optimal sensor set, although it has higher sensitivity than the cathode inlet flow, this indicates that the sensitivity alone is not enough for determination of optimal sensor set. Moreover, several temperatures can be included in the optimal sensor set (inlet/outlet temperatures at anode/cathode in Table 7) to replace the stack temperature, which cannot be measured directly in practical fuel cell system.

5.3. The proposed sensor selection approach

From above results, it can be seen that with only the sensitivity analysis, the optimal sensor set with minimum size cannot be obtained. On the other hand, the time-expensive exhaustive brute force searching method is not suitable in practical fuel cell system with many sensor candidates.

On this basis, the environment/measurement noise resistance of sensor is also used in the sensor selection process, and the optimal sensors will be determined based on the sensor sensitivity and noise resistance.

In this study, the noise resistance of sensors is evaluated based on the generated sensitivity matrix shown in Table 4, which can be express with Eq. (15).

$$\{\delta R\} = S\{\delta P\} \tag{15}$$

where S is the sensitivity matrix, $\{\delta R\}$ is the variation in sensor measurements, and $\{\delta P\}$ is the perturbations in health parameters.

With inversion of the sensitivity matrix S, the health parameter perturbation can be related through a gain matrix G to the sensor output variation by:

$$\{\delta P\} = \left(S^T S\right)^{-1} S^T \{\delta R\} = G\{\delta R\} \tag{16}$$

The evaluation of noise resistance of these sensors can be performed using Eq. (16). A set of (say n sets) response errors are generated randomly to express the measurement noise, which is a set of ±2% of the sensor measurements. With the subset of gain matrix G (formed using selected sensors), the corresponding health parameter errors (n sets) can be calculated using Eq. (16). From the health parameter errors, a statistical analysis is performed. For

Table 6
Available sensors from the fuel cell system.

Sensor	Symbol	Sensor	Symbol
Anode inlet temperature	Tin,an	Anode outlet pressure	Pout,an
Anode outlet temperature	Tout,an	Cathode inlet pressure	Pin,ca
Cathode inlet temperature	Tin,ca	Cathode outlet pressure	Pout,ca
Cathode outlet temperature	Tout,ca	Anode inlet flow	Win,an
Water inlet temperature	Tin,water	Anode outlet flow	Wout,an
Water outlet temperature	Tout,water	Cathode inlet flow	Win,ca
Anode inlet pressure	Pin,an	Cathode outlet flow	Wout,ca
Water inlet flow	Win,water	Cathode relative humidity	RH,ca

Table 8
Sensors with the best noise resistance capability from different sizes.

Size of sensor set	Sensor set with the best noise resistance capability
1	Stack temperature
2	Stack temperature, cathode outlet flow
3	Stack temperature, cathode outlet flow, cathode inlet flow
4	Stack temperature, cathode outlet flow, cathode inlet flow, water inlet temperature
5	Stack temperature, cathode outlet flow, cathode inlet flow, water inlet temperature, water outlet temperature
6	Stack temperature, cathode outlet flow, cathode inlet flow, water inlet temperature, water outlet temperature, anode outlet flow

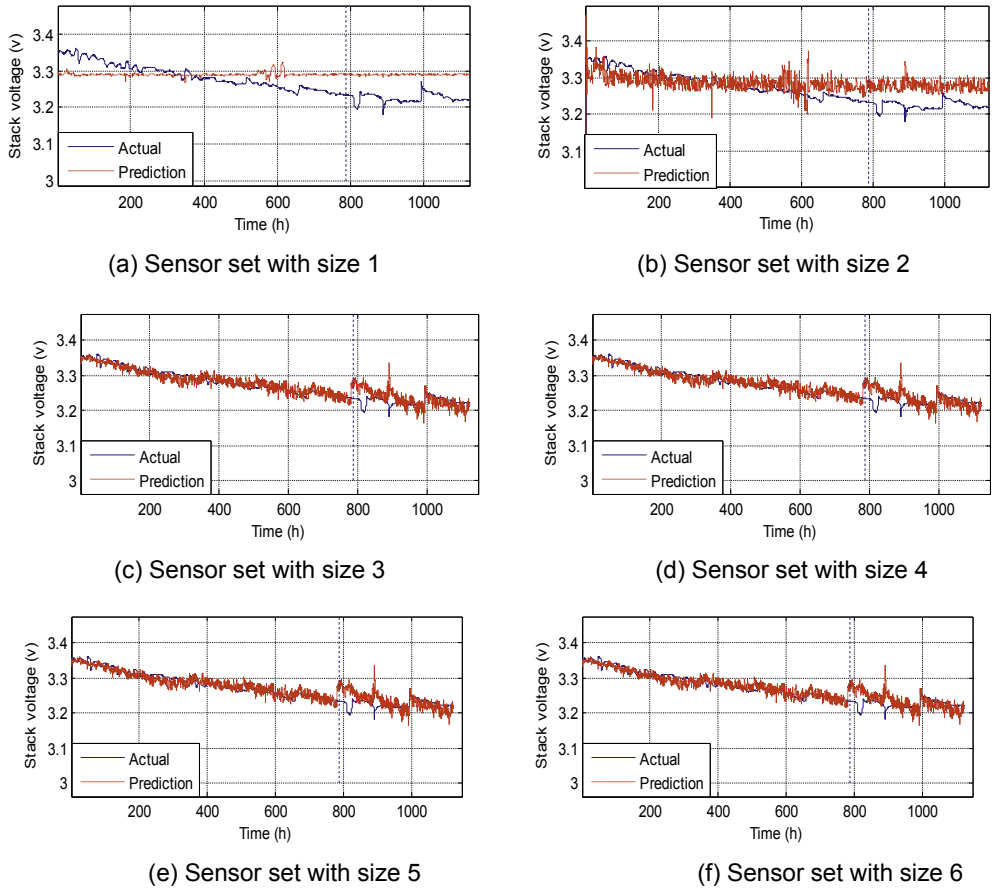

Fig. 6. Fuel cell prediction performance of various sensor sets (the vertical blue dashed line separates the training and validation stages). (For interpretation of the references to colour in this figure legend, the reader is referred to the web version of this article.)

example, the error for a particular parameter P_i is denoted as $\{\delta P_i\}$, which consists of n scalar components, the mean value μ_i and standard deviation σ_i are calculated from $\{\delta P_i\}$. Theoretically speaking, μ_i should be close to zero, thus the parameter error can be expressed usingσ_i. The index SD can be defined by including σ_i from errors of all the health parameters

$$SD = [\sigma_1 \ \sigma_2 \ldots \ \sigma_p] \tag{17}$$

where p represents the number of health parameters, and the overall error can be used to express the noise resistance of the selected sensor set (NR),

$$NR = \mu_{SD} + \sigma_{SD}/\mu_{SD} \tag{18}$$

Based on above results, the procedure of proposed sensor selection method can be proposed. With analysis results of fuel cell failure modes and their effects, the health parameters critical to the fuel cell performance can be determined. The sensitivity matrix

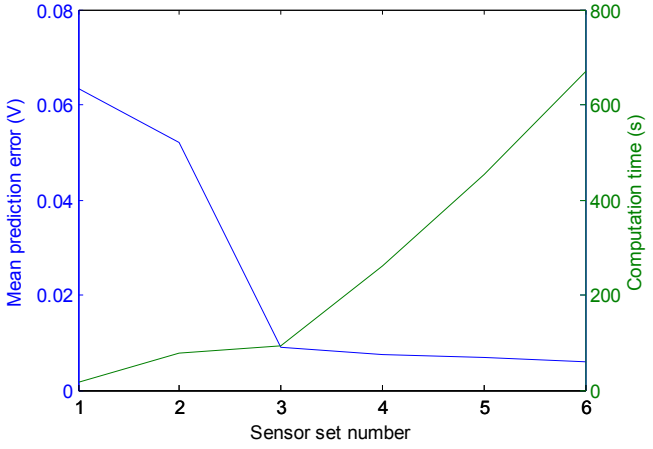

Fig. 7. Mean prediction error and computation cost of different sensor sets.

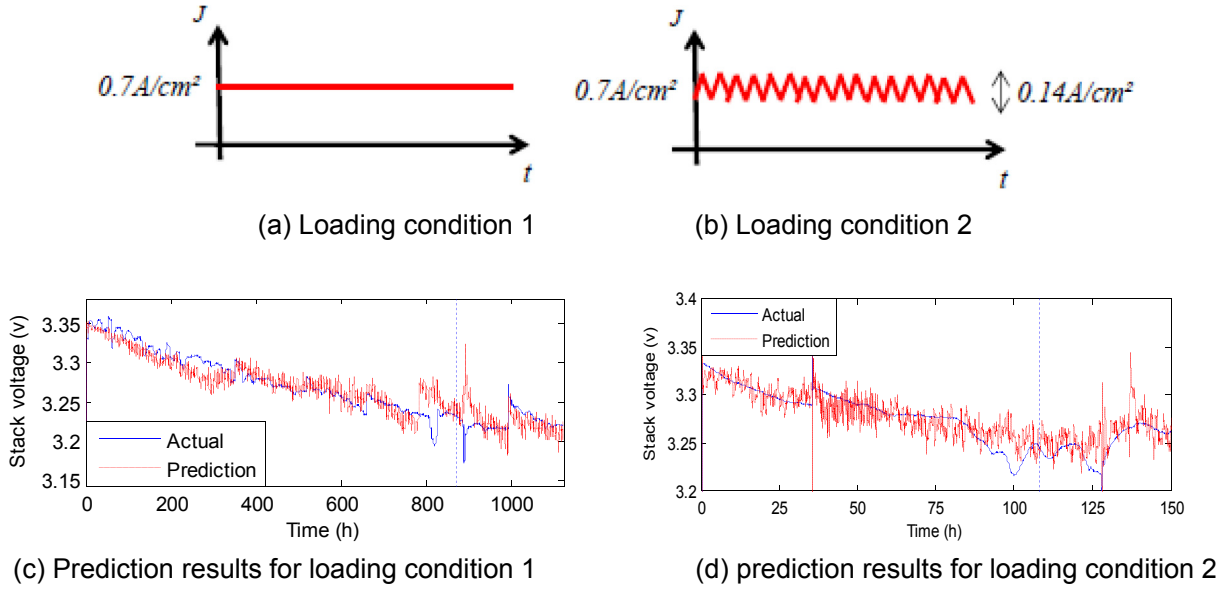

Fig. 8. Prediction results with selected sensors at different loading conditions (the vertical blue dashed line separates the training and validation stages).

between fuel cell health parameters and sensor measurements is then generated, with either the fuel cell model or test data. For sensor sets with different size, one sensor set is selected from each size using Eq. (18), which should have the best noise resistance capability. ANFIS is then used to evaluate the performance of these sensor sets, and the optimal sensor set can be determined based on the criteria that the fuel cell performance can be predicted with good quality using the minimum number of sensors.

Using Eq. (18), the noise resistance of various sensor sets can be evaluated, and the sensor set having the best noise resistance capability from each size can be determined, which are listed in Table 8. It should be mentioned that the cathode outlet temperature is used herein to replace the stack temperature in the table, which has been validated in section 5.2.

The performance of sensors set in Table 8 is evaluated using ANFIS, with similar procedure described in section 5.2, the fuel cell performance can be predicted with different sensor sets and the results are shown in Fig. 6. Moreover, the mean prediction error and computation time for each sensor set is depicted in Fig. 7.

From the results in Fig. 7 it can be seen that with increase of sensors, the prediction accuracy can be improved, when more than three sensors is used, the clearly prediction improvement cannot be observed, but the computation time is increased significantly. Therefore, from the proposed approach, the optimal sensor set with three sensors should be selected to predict the fuel cell performance.

However, it can be seen that from prediction results in Fig. 6, two points cannot be predicted (around 800 h and 900 h), even with increased number of sensors in the analysis. The reason is that at these points, sudden voltage drop is observed, which is due to disconnection of the load current, thus these points do not represent the aging process of the fuel cell system, and cannot be learned and predicted using ANFIS.

It should be noted that the proposed sensor selection algorithm only considers the prediction performance of sensors, while in practical fuel cell system, some other properties, including sensor reliability, sensor cost, and sensor transfer function, should also be included for the selection of sensors in the system, this can be performed by generating an objective function with these factors defined as constraints in the future work.

6. Capability of optimal sensors in predicting PEM fuel cell performance

In this section, the capability of optimal sensors in predicting fuel cell performance is studied using the test data from a PEM fuel cell system, more details about the test set-up and fuel cell test parameters can be found in Ref. [44]. In this study, two constant current loading conditions are selected for the analysis, which are depicted in Fig. 8(a) and (b), where constant current of 0.7 A/cm^2 is used in Fig. 8(a), and a constant current of 0.7 A/cm^2 with high frequency (5 kHz) current ripples (±10% of the constant value) is used in Fig. 8(b) [44].

Similar to the analysis in section 5.2, the ANFIS is used to predict the evolution of the fuel cell voltage using the optimal sensors. In the analysis, the same training/validation data sample ratio is used to train the ANFIS and predict fuel cell voltage, where the results are depicted in Fig. 8(c) and (d).

It can be observed that with optimal sensors, the trained ANFIS system can predict the fuel cell stack voltage with good quality at two different loading conditions, this can be seen from the mean prediction errors listed in Table 9. However, it should be noted that the maximum prediction error cannot be used to evaluate the performance of optimal sensors, since some valleys in fuel cell voltage curve cannot be learned and predicted correctly (voltages at about 800 h and 900 for the 1st loading condition, and voltages at about 100 h and 130 h for the 2nd loading condition), as they do not represent the actual fuel cell system aging process.

7. Conclusion

This paper investigates the sensor selection approaches for PEM fuel cell performance prediction, based on the sensitivity analysis.

Table 9
Mean prediction errors using optimal sensors at different loading currents.

Loading condition	Mean prediction error (V)
1	0.0089
2	0.0103

The optimal sensors can provide the reliable PEM fuel cell prediction performance with the minimum computation cost.

In the analysis, a numerical model of the fuel cell is developed and its performance is validated with test data. With the developed model, sensitivity matrix relating sensor measurements and fuel cell health parameters can be generated. Based on the sensitivity matrix, two approaches are applied to determine the optimal sensor set, including the largest gap method, and exhaustive brute force search method. From the results, a sensor selection approach is proposed to determine the optimal sensors, which considers both sensor sensitivity and noise resistance. Moreover, the prediction performance of optimal sensors is validated using test data from a PEM fuel cell system at different loading conditions. Results demonstrate that with optimal sensors, reliable fuel cell performance can be predicted with more effective computation cost. In the future work, the prediction performance of optimal sensors in dynamic loading condition will be investigated, which may consider the current variation effect in the selection process.

Acknowledgement

This work is supported by grant EP/K02101X/1 for Loughborough University, Department of Aeronautical and Automotive Engineering from the UK Engineering and Physical Sciences Research Council (EPSRC).Model and experimental data discussed in this work can be found at Loughborough Data Repository (https://lboro.figshare.com)

Appendix. List of symbols in PEM fuel cell model

Nomenclature

α	Charge transfer coefficient
A	Area (m^2)
C_{ps}	Specific heat capacity (J/kg.K)
E_n	Reversible cell voltage (V)
F	Faraday constant (C/mol)
h	Convective heat transfer coefficient ($W/m^2\ K$)
I	Stack current (A)
i	Current density (A/cm^2)
i_n	Internal current density (A/cm^2)
i_{oc}	Exchange current density at cathode (A/cm^2)
m	Mass (kg)
$\dot{m}$	Mass flow rate (kg/s)
m_{trans}	Mass transport loss coefficient
n_{trans}	Mass transport loss coefficient
Q	Heat energy (W)
R	Universal gas constant (J/mol.K)
$R_{membrane}$	Membrane resistance (Ω/cm^2)
T	Temperature (K)
T^0	Ambient temperature (K)
V	Voltage (V)
W	Mass flow rate (kg/s)

Subscript

act	From activation
elec	Electricity
FC	From fuel crossover
H_2	Hydrogen
H_2O	Water
in	Entering flow channels
liquid	Liquid
loss	Loss to surroundings
N_2	Nitrogen
O_2	Oxygen
ohm	From Ohmic
out	Existing flow channels
react	From reaction
stack	Fuel cell stack
trans	From transform
vapour	Vapour

References

[1] A. Forrai, H. Funato, Y. Yanagita, Y. Kato, Fuel-cell parameter estimation and diagnostics, IEEE Trans. Energy Convers. 20 (2005) 668–675.
[2] N. Fouquet, C. Doulet, C. Nouillant, G.D. Tanguy, B.O. Bouamama, Model based PEM fuel cell state-of-health monitoring via ac impedance measurements, J. Power Sources 159 (2006) 905–913.
[3] J.H. Ohs, U. Sauter, S. Maass, D. Stolten, Modeling hydrogen starvation conditions in proton exchange membrane fuel cells, J. Power Sources 196 (2011) 255–263.
[4] M.A. Rubio, A. Urquia, S. Dormido, Diagnosis of performance degradation phenomenon in PEM fuel cells, Int. J. Hydrogen Energy 35 (2010) 2586–2590.
[5] A. Zeller, O. Rallieres, J. Regnier, C. Turpin, Diagnosis of a hydrogen/air fuel cell by a statistical model-based method, in: Vehicle Power and Propulsion Conference (VPPC), Lille, France, 2010.
[6] M.M. Kamal, D. Yu, Model-based fault detection for proton exchange membrane fuel cell systems, Int. J. Eng. Sci. Technol. 3 (2011) 1–15.
[7] L.A.M. Riascos, M.G. Simoes, P.E. Miyagi, A Bayesian network fault diagnostic system for proton exchange membrane fuel cells, J. Power Sources 165 (2007) 267–278.
[8] L.A.M. Riascos, M.G. Simoes, P.E. Miyagi, On-line fault diagnostic system for proton exchange membrane fuel cells, J. Power Sources 175 (2008) 419–429.
[9] A. Mohammadi, A. Djerdir, D. Bouquain, B. Bouriot, D. Khaburi, Fault sensitive modeling and diagnosis of PEM fuel cell for automotive applications, in: Transportation Electrification Conference and Expo (ITEC), Detroit, 2013.
[10] R. Petrone, Z. Zheng, D. Hissel, M.C. Pera, C. Pianese, M. Sorrentino, M. Becherif, N. Yousfi-Steiner, A review on model-based diagnosis methodologies for PEMFCs, Int. J. Hydrogen Energy 38 (2013) 7077–7091.
[11] A. Narjiss, D. Depernet, D. Candusso, F. Custin, D. Hissel, Online diagnosis of PEM fuel cell, in: 13th Power Electronics and Motion Control Conference, Poznan, Poland, 2008.
[12] B. Legros, P.X. Thivel, Y. Bultel, M. Boinet, R.P. Nogueira, Accoustic emission: towards a real-time diagnosis technique for proton exchange membrane fuel cell operation, J. Power Sources 195 (2010) 8124–8133.
[13] L. Placca, R. Kouta, D. Candusso, J.F. Blachot, W. Charon, Analysis of PEM fuel cell experimental data using principle component analysis and multi linear regression, Int. J. Hydrogen Energy 35 (2010) 4582–4591.
[14] A. Taniguchi, T. Akita, K. Yasuda, Y. Miyazak, Analysis of electrocatalyst degradation in PEMFC caused by cell reversal during fuel starvation, J. Power Sources 130 (2011) 42–49.
[15] N.Y. Steiner, D. Hissel, P. Mocoteguy, D. Candusso, Non intrusive diagnosis of polymer electrolyte fuel cells by wavelet packet transform, Int. J. Hydrogen Energy 36 (2011) 740–746.
[16] J. Kim, J. Lee, Y. Tak, Relationship between carbon corrosion and positive electrode potential in a proton-exchange membrane fuel cell during start/stop operation, J. Power Sources 192 (2009) 674–678.
[17] J. Chen, B. Zhou, Diagnosis of PEM fuel cell stack dynamic behaviours, J. Power Sources 177 (2008) 83–95.
[18] E. Ramschak, V. Peinecke, P. Prenninger, T. Schaffer, V. Hacker, Detection of fuel cell critical status by stack voltage analysis, J. Power Sources 157 (2006) 837–840.
[19] M. Kim, N. Jung, K. Eorn, S.J. Yoo, J.Y. Kim, J.H. Jang, H.J. Kim, B.K. Hong, E. Cho, Effects of anode flooding on the performance degradation of polymer electrolyte membrane fuel cells, J. Power Sources 266 (2014) 332–340.
[20] Z. Zheng, R. Petrone, M.C. Pera, D. Hissel, M. Becherif, N.Y. Steiner, M. Sorrentino, A review on non-model based diagnosis methodologies for PEM fuel cell stacks and systems, Int. J. Hydrogen Energy 38 (2013) 8914–8926.
[21] J.G. Kim, S. Mukherjee, A. Bates, B. Zickel, S. Park, B.R. Son, J.S. Choi, O. Kwon, D.H. Lee, H.Y. Chung, Autocorrelation standard deviation and root mean square frequency analysis of polymer electrolyte membrane fuel cell to monitor for hydrogen and air undersupply, J. Power Sources 300 (2015) 164–174.
[22] Y. Vural, D.B. Ingham, M. Pourkashanian, Performance prediction of a proton exchange membrane fuel cell using the ANFIS model, Int. J. Hydrogen Energy 34 (2009) 9181–9187.
[23] S. Becker, V. Karri, Predictive models for PEM-electrolyzer performance using adaptive neuro-fuzzy inference systems, Int. J. Hydrogen Energy 35 (2010) 9963–9972.
[24] R.E. Silva, R. Gouriveau, S. Jemei, D. Hissel, L. Boulon, K. Agbossou, N.Y. Steiner, Proton exchange membrane fuel cell degradation prediction based on adaptive neuro-fuzzy inference systems, Int. J. Hydrogen Energy 39 (2014) 1–17.
[25] M. Jouin, R. Gouriveau, D. Hissel, M.C. Pera, N. Zerhouni, Prognostics of PEM fuel cell in a particle filtering framework, Int. J. Hydrogen Energy 39 (2013) 481–494.

[26] D.L. Simon, S. Garg, A systematic approach to sensor selection for aircraft engine health estimation, in: 19th ISABE Conference, Montreal, Canada, 2009.
[27] Y. Shuming, Q. Jing, L. Guanjun, Sensor optimization selection model based on testability constraint, Chin. J. Aeronautics 25 (2012) 262–268.
[28] A.M. William, K. George, M.S. Louis, S.S. Thomas, C. Amy, Sensor selection and optimization for health assessment of aerospace systems, J. Aerosp. Comput. Inf. Commun. 5 (2008) 16–34.
[29] L. Kehong, T. Xiaodong, L. Guanjun, Z. Chenxu, Sensor selection of helicopter transmission systems based on physical model and sensitivity analysis, Chin. J. Aeronautics 27 (2014) 643–654.
[30] A. Mawardi, R. Pitchumani, Effects of parameter uncertainty on the performance variability of proton exchange membrane (PEM) fuel cells, J. Power Sources 160 (2006) 232–245.
[31] L. Placca, R. Kouta, J. Blachot, W. Charon, Effects of temperature uncertainty on the performance of a degrading PEM fuel cell model, J. Power Sources 194 (2009) 313–327.
[32] G. Correa, F. Borello, M. Santarelli, Sensitivity analysis of temperature uncertainty in an aircraft PEM fuel cell, Int. J. Hydrogen Energy 36 (2011) 14745–14758.
[33] M. Noorkami, J. Robinson, Q. Meyer, O. Obeisun, E. Fraga, T. Reisch, Effects of temperature uncertainty on polymer electrolyte fuel cell performance, Int. J. Hydrogen Energy 39 (2014) 1439–1448.
[34] G. Correa, M. Santarelli, F. Borello, Sensitivity analysis of stack power uncertainty in a PEMFC-based powertrain for aircraft application, Int. J. Hydrogen Energy 40 (2015) 10354–10365.
[35] B. Rod, M. Jeremy, P. Bryan, S.K. Yu, M. Rangachary, G. Nancy, M. Deborah, W. Mahlon, G. Fernando, W. David, Z. Piotr, M. Karren, S. Ken, Z. Tom, B. James, E.M. James, I. Minoru, M. Kenji, H. Michio, O. Kenichiro, O. Zempachi, M. Seizo, N. Atsushi, S. Zyun, U. Yoshiharu, Y. Kazuaki, K. Ken-ichi, I. Norio, Scientific aspects of polymer electrolyte fuel cell durability and degradation, Chem. Rev. 107 (2007) 3904–3951.
[36] J. Wu, X.Z. Yuan, J.J. Martin, H. Wang, J. Zhang, J. Shen, S. Wu, W. Merida, A review of PEM fuel cell durability: degradation mechanisms and mitigation strategies, J. Power Sources 184 (2008) 104–119.
[37] M. Knowles, D. Baglee, A. Morris, Q. Ren, The state of art in fuel cell condition monitoring and maintenance, in: 25th World Electric Vehicle Symposium and Exposition, Shenzhen, China, 2010.
[38] M. Jouin, R. Gouriveau, D. Hissel, M.C. Pera, N. Zerhouni, Degradations analysis and aging modeling for health assessment and prognostics of PEMFC, Reliab. Eng. Syst. Saf. 148 (2016) 78–95.
[39] J.M.L. Canut, R.M. Abouatallah, D.A. Harrington, Detection of membrane dying, fuel cell flooding, and anode catalyst poisoning on PEMFC stacks by electrochemical impedance spectroscopy, J. Electrochem. Soc. 153 (2006) 857–864.
[40] J.T. Pukrushpan, Modeling and Control of Fuel Cell Systems and Fuel Processors, Doctoral dissertation, The University of Michigan, USA, 2003.
[41] T. Selyari, A.A. Ghoreyshi, M. Shakeri, G.D. Najafpour, T. Jafary, Measurement of polarization curve and development of a unique semi-empirical model for description of PEMFC and DMFC performances, Chem. Industry Chem. Eng. Q. 17 (2011) 207–214.
[42] T. Ous, C. Arcoumanis, Degradation aspects of water formation and transport in proton exchange membrane fuel cell: a review, J. Power Sources 240 (2013) 558–582.
[43] A.P. Engelbrecht, A new pruning heuristic based on variance analysis of sensitivity information, IEEE Trans. Neural Netw. 12 (2001) 1386–1399.
[44] FCLAB research, IEEE PHM Data Challenge 2014, 2014. http://eng.fclab.fr/ieee-phm-2014-data-challenge/.